Sequential solvation of HCl in argon: High resolution infrared spectroscopy of Ar n HCl (n=1,2,3)

David T. Anderson, Scott Davis, and David J. Nesbitt

Citation: The Journal of Chemical Physics **107**, 1115 (1997); doi: 10.1063/1.474458
View online: http://dx.doi.org/10.1063/1.474458
View Table of Contents: http://scitation.aip.org/content/aip/journal/jcp/107/4?ver=pdfcov
Published by the AIP Publishing

Sequential solvation of HCl in argon: High resolution infrared spectroscopy of Ar_nHCl ($n=1,2,3$)

David T. Anderson, Scott Davis, and David J. Nesbitt[a)]
JILA, University of Colorado and National Institute of Standards and Technology, and Department of Chemistry and Biochemistry, University of Colorado Boulder, Colorado 80309-0440

(Received 10 March 1997; accepted 28 March 1997)

High-resolution near-infrared spectra of the $v_{HCl}=1\leftarrow 0$ fundamental stretch in Ar_2HCl and Ar_3HCl have been characterized using a slit-jet infrared spectrometer. Analysis of the jet-cooled, rotationally resolved spectra (i) permits unambiguous identification of the cluster size, (ii) provides vibrationally averaged geometries in the $v_{HCl}=1$ excited state, and (iii) allows the vibrational shift of the HCl chromophore to be measured as a function of the number of Ar atoms in the complex. The equilibrium structures of Ar_nHCl ($n=1-3$) clusters calculated using accurate Ar–Ar and Ar–HCl pair potentials are consistent with the vibrationally averaged structures inferred spectroscopically. The vibrational red-shifts for Ar_nHCl ($n=1-3$) reflect a near-*linear* dependence on the number of Ar atoms, which is qualitatively reproduced by simple classical calculations on $v_{HCl}=0$ and 1 pairwise additive potential surfaces. Theoretical predictions of the Ar_nHCl red-shifts in a fcc lattice indicate good agreement with experimental matrix results. However, to achieve this asymptotic limit requires up to $n\approx 54$ Ar atoms; this underscores a clear sensitivity to *non*-nearest neighbor Ar–HCl interactions significantly *outside* the first solvation shell. Finally, for smaller Ar_nHCl clusters with only one solvation shell ($n=12$), the potentials predict an energetic preference for HCl in *surface* vs *interior* sites. Analysis indicates that this effect is predominantly due to Ar/HCl size mismatch, which destabilizes the nearest neighbor Ar shell for HCl solvated in the center of the cluster. © *1997 American Institute of Physics.* [S0021-9606(97)01825-4]

I. INTRODUCTION

The idea that the properties of condensed matter are ultimately determined by the cumulative pairwise and nonpairwise forces between the constituent molecules or atoms is a powerfully appealing intuitive picture. Though difficult to achieve in practice, this simple picture is at the heart of any theory of microscopic solvation phenomena in both cluster and condensed phases. Indeed, one long-standing experimental challenge in the cluster community has been to develop detailed spectroscopic methods that can isolate and probe these intermolecular interactions as a function of size, starting first with simple pairs and sequentially adding molecules until the macroscopic limit is eventually reached.[1,2] Though the field is still far from achieving this limit, a tremendous amount of detailed information about intermolecular forces between pairs of molecules has been obtained by high resolution spectroscopic studies of dimers. When combined with modern quantum theoretical methods, such spectroscopic studies have emerged as an extremely powerful tool for characterizing true pairwise interactions and have resulted in quantitatively accurate potentials for several systems such as Ar–HCl,[3] Ar–HF,[4] Ar–H_2,[5] Ar–H_2O,[6] and Ar–NH_3.[7]

The clear interest in much larger clusters raises new and challenging issues of many body intermolecular contributions to the full potential surface. The basic question can be simply stated; given accurate two-body (i.e., pair) potentials, how well are the interactions of larger ensembles of molecules described by a sum over all possible pairwise interactions? Since an essential prerequisite to addressing this issue rigorously is a quantitatively reliable pair potential, this has been a difficult question to pose, both experimentally and theoretically. Furthermore, the extent to which this ''pairwise additive'' approximation adequately describes intermolecular forces in clusters varies considerably from system to system; consequently, a study of multiple systems may be necessary to elucidate the correct features of the nonpairwise additive contributions. One clear goal of such studies has been to develop the ability to modify pair potentials by sums over the necessary n-body terms, and thereby provide access to accurate potential energy surfaces for describing arbitrarily large clusters up to and including the condensed phase limit. Though the full fruition of such efforts remains in the future, there have recently been important successes in model systems that indicate significant progress along this path.

One prototypic system that has been particularly revealing for both spectroscopic characterization and theoretical modeling of multibody forces are the complexes formed between a single hydrogen halide and multiple rare gas Ar atoms. From an experimental standpoint, early microwave experiments by Gutowsky and co-workers on the Ar_nHF/DF($n=1-4$) (Refs. 8–10) and Ar_nHCl/DCl($n=1-3$) (Refs. 11,12) oligomers clearly demonstrated how such a series of cluster sizes could be ''synthesized'' under supersonic jet conditions and studied in considerable spectroscopic detail. Specifically, these microwave experiments provided information with which to characterize vibra-

[a)]Staff member, Quantum Physics Division, National Institute of Standards and Technology.

tionally averaged structures for each cluster in the series. Far-IR spectroscopic studies by Elrod *et al.* extended this to vibrationally excited levels, characterizing three intermolecular bending states for Ar_2HCl (Refs. 13–15) and one in Ar_2DCl.[16] Analogous studies of in-plane and out-of-plane bending states in Ar_2HF/DF have recently been conducted via inter-+intra-molecular combination band excitation by Farrell and Nesbitt[17] in the near-IR. Both the near- and far-infrared studies are particularly valuable since direct excitation of the ''soft'' intermolecular modes provides access to substantially larger regions of the anisotropic angular-radial intermolecular potential. In addition, both Ar_nHF ($n=1-4$) (Ref. 18) and Ar_nDF ($n=1-3$) (Ref. 19) have been studied in the near-IR via excitation of the intramolecular $v_{HX/DX}=1$ stretch. Of special importance to the present work, these studies also determined the ''red-shift'' in the HX vibrational frequency induced by complex formation, which is sensitive to the number and vibrationally averaged structure of the ''solvent'' Ar atoms.

The Ar_nHX complexes are also particularly accessible from the standpoint of rigorous theoretical calculations. The Ar–Ar pair potential has been the benchmark atom–atom potential for over 30 years, with the most recent and highly accurate versions determined from a combination of crossed beam scattering and UV spectroscopic studies.[20] Arguably the most accurate atom–molecule potentials are the Ar–HCl and Ar–HF potentials developed by Hutson and co-workers[3,4] from inversion of a large body of high resolution ArHX spectroscopic data. Thus, approximate potentials for HCl ''solvated'' in an arbitrary number of Ar atoms can be constructed simply by summing over all the pairwise interactions. In principle, solving the multidimensional intermolecular quantum mechanics for nuclear motion on this potential provides a rigorously predictive framework for Ar_nHCl complexes at the pairwise additive level, which can therefore be used to probe for nonpairwise additive effects. Indeed, Hutson and co-workers[21] have performed close coupling calculations for Ar_2HCl/DCl that explicitly include all intermolecular coordinates, with the high frequency stretching coordinate included parametrically as a function of v_{HCl}. A comparison of the rotational constants and vibrational frequencies calculated on the pairwise additive potential have identified significant discrepancies with experiment that are attributable to nonadditive terms in the full potential surface. Several nonadditive contributions have been investigated, from which it was found that additional terms accounting for three-body dispersion, induction, and exchange interactions are necessary to bring the calculated results into good agreement with experiment.

Another experimental observable which can be provided by near-infrared studies of the Ar_nHCl family is the shift in the vibrational frequency of the HCl chromophore. This shift is quite sensitive to the local structure of the Ar atoms around the HCl. High resolution rotationally resolved spectra allow the size of the cluster to be determined unambiguously, which permits the redshift to be studied as a function of the number of Ar atoms in the complex.[18,19] At the other extreme, the vibrational red-shift can also be determined accurately under rare gas matrix isolation conditions,[22,23] i.e., effectively in the limit of an infinite number of solvation shells. Vibrational red-shifts in these intermediate size clusters, therefore, potentially offer a quantitative link between the study of dimers and bulk condensed phase phenomena.

In the present work, we employ high resolution infrared absorption spectroscopy to vibrationally excite the HCl moiety in Ar_2HCl and Ar_3HCl. Analysis of the resulting rotationally resolved spectra allows us to size-select the different clusters formed in a slit jet expansion. For each cluster the rotational constants are used to infer the vibrationally averaged structure in the HCl stretch excited state. These structures can be compared with those determined for the ground intramolecular state from microwave and far-IR spectra to quantify the effect of vibrational excitation of the HCl chromophore. To make a more direct comparison with this experimental data, we also take advantage of the well determined Ar–Ar and Ar–HCl pair potentials to construct a multidimensional pairwise additive potential for Ar_nHCl clusters. In conjunction with classical energy minimization methods, we theoretically examine the equilibrium structures of much larger Ar_nHCl ($n\leqslant 54$)) clusters and the vibrational red-shift for HCl embedded in large ensemble lattices of Ar atoms intended to mimic the relevant cage sizes and internal forces in bulk solid Ar environment.

The remainder of this paper is organized as follows. Section II describes the experimental apparatus and Sec. III presents the spectroscopic results and analysis. Section IV describes the inertial analysis of the molecular constants used to infer vibrationally averaged geometries. The Ar_nHCl pairwise additive potential is used to predict equilibrium structures and classical red-shifts which are compared with experiment for the small clusters. This is followed by a more quantitative comparison of the experimental data with diffusion quantum Monte Carlo calculations by Lewerenz.[24] Finally, classical redshift calculations are performed for HCl in a relaxed Ar fcc lattice ($n\leqslant 54$) as a function of shell size and compared with matrix isolation results. Section V summarizes our conclusions and describes directions for future work.

II. EXPERIMENT

The Ar_nHCl complexes are formed by adiabatically expanding mixtures of 0.5% HCl in a 50–50 mix of Ar and ''welding grade Ne'' (70% Ne, 30% He), at a backing pressure of 450 Torr, through a 4 cm×190 μm pulsed slit jet. Infrared spectra of the complexes are recorded utilizing timegated, dual beam direct infrared absorption detection. Narrow bandwidth (2 MHz) infrared light is generated via nonlinear mixing of a single mode, fixed frequency Ar^+ laser (514.5 nm) and a single mode, tunable ring dye laser operating on R6G. Multipass optics are used to pass the infrared light 20 times through the expansion for a total absorption path length of 80 cm.

The single frequency Ar^+ laser is frequency stabilized to a transfer cavity that is actively locked to a polarization stabilized HeNe laser. The transmission fringes obtained by

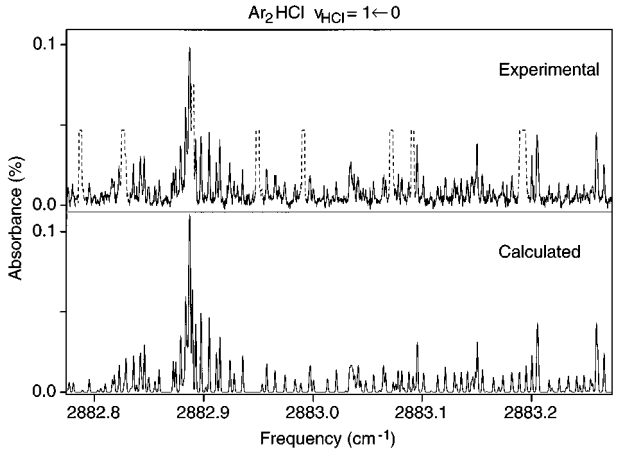

FIG. 1. Experimental and calculated spectra for $Ar_2H^{35}Cl$ near the band origin. The calculated spectrum is generated using the constants in Table III, obtained from a least squares fit of the experimental data. The dotted line peaks in the experimental spectrum are transitions due to $ArH^{35}Cl$, $ArH^{37}Cl$, and $(HCl)_2$, and have been suppressed to highlight the $Ar_2H^{35}Cl$ structure.

scanning the dye laser are also recorded with the transfer cavity to permit the measurement of relative frequencies to a precision better than 0.0001 cm^{-1}. This frequency precision proves invaluable for the assignment and analysis of the spectra of the Ar_nHCl ($n=1,2,3$) clusters since the rotational constants are already quite small ($B\approx 0.05$ cm^{-1}) and this region of the spectrum is heavily congested with strong transitions due to both $ArH^{35}Cl/ArH^{37}Cl$ isotopomers as well as $(HCl)_2$. Absolute frequency calibration is made with respect to the $P(16)$ transition (2882.3036 cm^{-1}) of the $ArH^{35}Cl$ fundamental.[25] This calibration procedure allows the transition frequencies and vibrational origins to be reported to an absolute accuracy of 0.0002 cm^{-1}.

III. RESULTS AND ANALYSIS

A. Ar_2HCl

Previous analyses by Gutwosky and co-workers[11] in the microwave, and by Saykally and co-workers[13–15] in the far-IR, have indicated that the equilibrium geometry of Ar_2HCl is T-shaped, with the HCl pointing along the C_2 symmetry axis of the complex. The transition moment for excitation of the HCl stretch lies along the a inertial axis, and consequently excitation of the $v_{HCl}=1\leftarrow 0$ near-IR fundamental should result in an A type band with asymmetric top structure and a strong central Q-branch. In good qualitative agreement with these expectations, there are two features characteristic of an asymmetric top Q-branch, separated by approximately 2.1 cm^{-1} with the feature to the blue approximately three times stronger in intensity. The frequency separation and relative intensities of these two features are consistent with the two isotopomers expected for a complex containing a single HCl molecule, with $H^{35}Cl$ and $H^{37}Cl$ present in 3:1 natural abundance. Figure 1 shows a sample 0.5 cm^{-1} scan region around the Q-branch feature assigned to the $Ar_2H^{35}Cl$ isotopomer, demonstrating the exceedingly dense spectral structure due to the trimer species.

The rotational structure for both isotopomers is readily assigned using ground state combination differences calculated from the rotational constants determined by Elrod *et al.*,[15] and permits unambiguous labeling of the lower $J_{K_aK_c}$ rotational quantum numbers. This method of assignment takes maximum advantage of the high frequency precision of the spectrometer (~5 MHz), which proves essential due to the high density of lines in the spectrum even under 5–10 K slit jet expansion conditions. The root mean square (rms) deviation between observed and calculated combination differences is ≈6 MHz, i.e., consistent with the experimental uncertainty. Furthermore, since rotation about the a inertial axis (i.e., the C_2 axis) for the Ar_2HCl complex involves exchange of identical boson nuclei (^{40}Ar with $I=0$), nuclear spin constraints on the total wave function restrict K_a to even non-negative integers in the ground state. Thus the assignment can be additionally confirmed by the complete absence of transitions out of $K_a=1,3,5,\ldots$ lower levels. Infrared selection rules identify this as an A type band (i.e., $\Delta K_a=0,\pm 2,\ldots$, $\Delta K_c=\pm 1,\pm 3,\ldots$), which is consistent with a vibrational transition moment along the Ar_2–HCl intermolecular axis. The observed transition frequencies are listed in Tables I and II for the $Ar_2H^{35}Cl$ and $Ar_2H^{37}Cl$ isotopomer species, respectively.

The infrared data for both isotopomers can be well fit to a S-reduction, III^r representation Watson asymmetric top Hamiltonian.[26] All near-IR data are consistent with the previously determined ground state constants,[15] which are therefore held fixed in the spectral fits. Fitted molecular constants for both isotopomers are reported in Table III. The rms deviation of the $Ar_2H^{35}Cl$ and $Ar_2H^{37}Cl$ fits are 0.000 17 and 0.000 18 cm^{-1}, respectively, again comparable to or greater than the 0.0001 cm^{-1} experimental precision. A comparison of the experimental data with a simulated spectrum generated using the constants from the fit is shown in Fig. 1 for $Ar_2H^{35}Cl$, corroborating the assignment and demonstrating the high quality of the fit. The band origin for $Ar_2H^{35}Cl$ is 2 882.751 76(3) cm^{-1}, i.e., red-shifted 3.2236 cm^{-1} from the uncomplexed $H^{35}Cl$ origin, and approximately twice as large as the 1.7667 cm^{-1} shift for a single Ar atom in ArHCl.[25] The nearly linear dependence of the red-shift on the number of Ar atoms is substantially different from the much more nonlinear n dependencies measured[17–19] for both Ar_nHF and Ar_nDF, i.e., where the incremental red-shift decreases with successive Ar atoms. We will return to the possible reasons for this discrepancy in greater detail in the Discussion.

B. Ar_3HCl

With the Ar_2HCl transitions satisfactorily assigned, we are in a position to interrogate the much less intense additional features due to larger clusters. Indeed, only after all the Ar_2HCl transitions were identified and assigned did an unassigned weak feature at ~2881.45 cm^{-1} become evident. This feature is shown in Fig. 2 where at the top of the figure

TABLE I. Transition frequencies (cm^{-1}): $v_{HCl}=1\leftarrow0$ a-type stretch excitation in $Ar_2H^{35}Cl$.

$J'_{K'_a,K'_c}\leftarrow J''_{K''_a,K''_c}$	Frequency $(o-c)$	$J'_{K'_a,K'_c}\leftarrow J''_{K''_a,K''_c}$	Frequency $(o-c)$
$21_{0,21}\leftarrow 20_{0,20}$	2 883.888 56	$4_{0,4}\leftarrow 3_{0,3}$	2 883.001 81
$20_{0,20}\leftarrow 19_{0,19}$	2 883.838 85	$7_{4,4}\leftarrow 7_{2,5}$	2 882.992 82
$11_{8,3}\leftarrow 10_{8,2}$	2 883.822 30	$8_{4,4}\leftarrow 8_{4,5}$	2 882.987 28
$12_{8,5}\leftarrow 11_{8,4}$	2 883.807 46	$9_{6,4}\leftarrow 9_{4,5}$	2 882.981 16
$13_{6,7}\leftarrow 12_{6,6}$	2 883.803 53	$10_{6,4}\leftarrow 10_{6,5}$	2 882.972 85
$14_{6,9}\leftarrow 13_{6,8}$	2 883.799 83	$11_{8,4}\leftarrow 11_{6,5}$	2 882.965 74
$19_{0,19}\leftarrow 18_{0,18}$	2 883.788 58	$3_{0,3}\leftarrow 2_{0,2}$	2 882.947 00
$13_{6,8}\leftarrow 12_{6,7}$	2 883.749 66	$2_{0,2}\leftarrow 1_{0,1}$	2 882.892 64
$14_{4,10}\leftarrow 13_{4,9}$	2 883.746 45	$1_{0,1}\leftarrow 0_{0,0}$	2 882.834 82
$15_{4,12}\leftarrow 14_{4,11}$	2 883.743 63		
$16_{2,14}\leftarrow 15_{2,13}$	2 883.741 40	$0_{0,0}\leftarrow 1_{0,1}$	2 882.667 52
$18_{0,18}\leftarrow 17_{0,17}$	2 883.739 05	$3_{0,3}\leftarrow 4_{0,4}$	2 882.495 66
$12_{6,7}\leftarrow 11_{6,6}$	2 883.699 27	$2_{2,0}\leftarrow 3_{2,1}$	2 882.445 02
$14_{4,11}\leftarrow 13_{4,10}$	2 883.693 32	$4_{0,4}\leftarrow 5_{0,5}$	2 882.438 06
$17_{0,17}\leftarrow 16_{0,16}$	2 883.688 43	$5_{0,5}\leftarrow 6_{0,6}$	2 882.380 01
$16_{2,15}\leftarrow 15_{2,14}$	2 883.688 43	$3_{2,1}\leftarrow 4_{2,2}$	2 882.374 11
$10_{6,4}\leftarrow 9_{6,3}$	2 883.654 10	$6_{0,6}\leftarrow 7_{0,7}$	2 882.321 71
$11_{6,6}\leftarrow 10_{6,5}$	2 883.648 34	$4_{2,2}\leftarrow 5_{2,3}$	2 882.321 71
$11_{4,7}\leftarrow 10_{4,6}$	2 883.593 89	$4_{4,1}\leftarrow 5_{4,2}$	2 882.278 82
$12_{4,9}\leftarrow 11_{4,8}$	2 883.591 10	$7_{0,7}\leftarrow 8_{0,8}$	2 882.263 05
$8_{6,2}\leftarrow 7_{6,1}$	2 883.550 65	$5_{2,3}\leftarrow 6_{2,4}$	2 882.263 15
$9_{6,4}\leftarrow 8_{6,3}$	2 883.545 34	$4_{4,0}\leftarrow 5_{4,1}$	2 882.226 18
$10_{4,6}\leftarrow 9_{4,5}$	2 883.542 42	$5_{4,2}\leftarrow 6_{4,3}$	2 882.208 07
$11_{4,8}\leftarrow 10_{4,7}$	2 883.539 67	$8_{0,8}\leftarrow 9_{0,9}$	2 882.204 43
$12_{2,10}\leftarrow 11_{2,9}$	2 883.537 35	$6_{2,4}\leftarrow 7_{2,5}$	2 882.204 43
$14_{0,14}\leftarrow 13_{0,13}$	2 883.534 76	$9_{0,9}\leftarrow 10_{0,10}$	2 882.145 39
$13_{2,12}\leftarrow 12_{2,11}$	2 883.534 76	$7_{2,5}\leftarrow 8_{2,6}$	2 882.145 39
$9_{4,5}\leftarrow 8_{4,4}$	2 883.490 43	$5_{4,1}\leftarrow 6_{4,2}$	2 882.136 94
$10_{4,7}\leftarrow 9_{4,6}$	2 883.487 95	$10_{0,10}\leftarrow 11_{0,11}$	2 882.085 93
$11_{2,9}\leftarrow 10_{2,8}$	2 883.485 57	$8_{2,6}\leftarrow 9_{2,7}$	2 882.085 93
$13_{0,13}\leftarrow 12_{0,12}$	2 883.483 10	$6_{4,2}\leftarrow 7_{4,3}$	2 882.081 06
$6_{6,0}\leftarrow 5_{4,1}$	2 883.476 95	$6_{6,1}\leftarrow 7_{6,2}$	2 882.061 84
$7_{6,1}\leftarrow 6_{6,0}$	2 883.459 82	$11_{0,11}\leftarrow 12_{0,12}$	2 882.026 33
$8_{4,4}\leftarrow 7_{4,3}$	2 883.439 56	$9_{2,7}\leftarrow 10_{2,8}$	2 882.026 33
$9_{4,6}\leftarrow 8_{4,5}$	2 883.435 98	$8_{4,5}\leftarrow 9_{4,6}$	2 882.026 33
$10_{2,8}\leftarrow 9_{2,7}$	2 883.433 56	$7_{4,3}\leftarrow 8_{4,4}$	2 882.026 33
$12_{0,12}\leftarrow 11_{0,11}$	2 883.431 07	$6_{6,0}\leftarrow 7_{6,1}$	2 882.014 35
$7_{4,3}\leftarrow 6_{4,2}$	2 883.389 86	$7_{6,2}\leftarrow 8_{6,3}$	2 881.978 45
$8_{4,5}\leftarrow 7_{4,4}$	2 883.383 36	$12_{0,12}\leftarrow 13_{0,13}$	2 881.966 41
$9_{2,7}\leftarrow 8_{2,6}$	2 883.380 89	$10_{2,8}\leftarrow 11_{2,9}$	2 881.966 41
$11_{0,11}\leftarrow 10_{0,10}$	2 883.378 38	$8_{6,3}\leftarrow 9_{6,4}$	2 881.911 24
$6_{4,2}\leftarrow 5_{4,1}$	2 883.338 92	$9_{4,5}\leftarrow 10_{4,6}$	2 881.908 51
$8_{2,6}\leftarrow 7_{2,5}$	2 883.328 21	$13_{0,13}\leftarrow 14_{0,14}$	2 881.906 19
$10_{0,10}\leftarrow 9_{0,9}$	2 883.325 64	$11_{2,9}\leftarrow 12_{2,10}$	2 881.906 19
$7_{2,5}\leftarrow 6_{2,4}$	2 883.275 56	$7_{6,1}\leftarrow 8_{6,2}$	2 881.901 90
$6_{4,3}\leftarrow 5_{4,2}$	2 883.275 56	$10_{4,6}\leftarrow 11_{4,7}$	2 881.848 27
$9_{0,9}\leftarrow 8_{0,8}$	2 883.272 57	$14_{0,14}\leftarrow 15_{0,15}$	2 881.845 67
$5_{4,1}\leftarrow 4_{4,0}$	2 883.260 52	$12_{2,10}\leftarrow 13_{2,11}$	2 881.845 67
$12_{4,9}\leftarrow 12_{2,10}$	2 883.257 13	$8_{6,2}\leftarrow 9_{6,3}$	2 881.835 20
$13_{4,9}\leftarrow 13_{4,10}$	2 883.248 47	$11_{4,7}\leftarrow 12_{4,8}$	2 881.787 49
$6_{2,4}\leftarrow 5_{2,3}$	2 883.221 79	$15_{0,15}\leftarrow 16_{0,16}$	2 881.784 62
$8_{0,8}\leftarrow 7_{0,7}$	2 883.219 03	$13_{2,11}\leftarrow 14_{2,12}$	2 881.784 62
$5_{4,2}\leftarrow 4_{4,1}$	2 883.214 21	$16_{0,16}\leftarrow 17_{0,17}$	2 881.723 02
$11_{4,8}\leftarrow 11_{2,9}$	2 883.205 15	$14_{2,12}\leftarrow 15_{2,13}$	2 881.723 02
$12_{4,8}\leftarrow 12_{4,9}$	2 883.196 78	$17_{0,17}\leftarrow 18_{0,18}$	2 881.662 34
$5_{2,3}\leftarrow 4_{2,2}$	2 883.168 99	$15_{2,13}\leftarrow 16_{2,14}$	2 881.662 34
$9_{2,7}\leftarrow 9_{2,8}$	2 883.159 42	$18_{0,18}\leftarrow 19_{0,19}$	2 881.600 65
$10_{4,7}\leftarrow 10_{2,8}$	2 883.152 54	$16_{2,14}\leftarrow 17_{2,15}$	2 881.600 65
$11_{4,7}\leftarrow 11_{4,8}$	2 883.144 82	$19_{0,19}\leftarrow 20_{0,20}$	2 881.538 89
$4_{2,2}\leftarrow 3_{2,1}$	2 883.118 26	$17_{2,15}\leftarrow 18_{2,16}$	2 881.538 89
$6_{0,6}\leftarrow 5_{0,5}$	2 883.111 22	$20_{0,20}\leftarrow 21_{0,21}$	2 881.476 82
$15_{8,7}\leftarrow 15_{8,8}$	2 883.107 50	$18_{2,16}\leftarrow 19_{2,17}$	2 881.476 82
$9_{4,6}\leftarrow 9_{2,7}$	2 883.099 72	$21_{0,21}\leftarrow 22_{0,22}$	2 881.414 30

TABLE I. (*Continued*).

$J'_{K'_a,K'_c}\leftarrow J''_{K''_a,K''_c}$	Frequency $(o-c)$	$J'_{K'_a,K'_c}\leftarrow J''_{K''_a,K''_c}$	Frequency $(o-c)$
$10_{4,6}\leftarrow 10_{4,7}$	2 883.092 88	$19_{2,17}\leftarrow 20_{2,18}$	2 881.414 30
$11_{6,6}\leftarrow 11_{4,7}$	2 883.085 40	$22_{0,22}\leftarrow 23_{0,23}$	2 881.351 74
$12_{6,6}\leftarrow 12_{6,7}$	2 883.076 78	$20_{2,18}\leftarrow 21_{2,19}$	2 881.351 74
$13_{8,6}\leftarrow 13_{6,7}$	2 883.067 81	$23_{0,23}\leftarrow 24_{0,24}$	2 881.288 81
$5_{0,5}\leftarrow 4_{0,4}$	2 883.056 87	$24_{0,24}\leftarrow 25_{0,25}$	2 881.225 77
$3_{2,1}\leftarrow 2_{2,0}$	2 883.051 91	$25_{0,25}\leftarrow 26_{0,26}$	2 881.162 31
$10_{6,5}\leftarrow 10_{4,6}$	2 883.033 72	$26_{0,26}\leftarrow 27_{0,27}$	2 881.098 78
$11_{6,5}\leftarrow 11_{6,6}$	2 883.025 30		
$13_{8,5}\leftarrow 13_{8,6}$	2 883.006 60		

the experimentally measured spectrum is shown. Directly below the experimental spectrum is a model Ar_2HCl spectrum generated from the constants in Table III. Since in this region of the spectrum transitions due to both $Ar_2H^{35}Cl$ and $Ar_2H^{37}Cl$ are present, the model spectrum is a convolution of the spectra for both isotopomers weighted by the 3:1 natural abundance of ^{35}Cl:^{37}Cl. After subtracting the calculated spectrum from the experimental data [as well as three relatively strong features due to $ArH^{37}Cl$, $ArH^{35}Cl$, and $(HCl)_2$], the unaccounted for feature at 2881.46 cm^{-1} becomes more apparent (see Fig. 2). Indeed, a similar type of analysis throughout the spectrum convincingly displays the excellent modeling of the Ar_2HCl features that enable their contribution to the observed spectrum to be effectively extracted.

Based on the previous microwave studies of Gutwosky and co-workers,[12] the equilibrium geometry of the Ar_3HCl tetramer has C_{3v} symmetry, with the HCl pointing along the C_3 symmetry axis. The HCl monomer lies along the symmetric top axis indicating that the near-IR $v_{HCl}=1\leftarrow0$ fundamental should be a parallel band ($\Delta K=0$). The three equivalent Ar atoms with nuclear spin $I=0$ limits the available quantum states by Bose–Einstein statistics, such that only $K=0$, ±3, ±6,... states have nonzero statistical weights in the ground vibrational state. The unassigned feature is characteristic of the central Q-branch of a symmetric top and thus used as a guide for a search for additional P/R transitions. Using $Ar_3H^{35}Cl$ combination differences calculated from the microwave molecular constants, nearly perfectly overlapping transitions out of $K=0$, ±3 in the P/R-branch were assigned centered around the suspected Q-branch feature. Even higher K states could also be assigned using ground state combination differences for approximately 10 transitions. The P/R-branch structure is fit to a symmetric top Hamiltonian,

$$E=BJ(J+1)+(A-B)K^2-D_JJ(J+1)^2-D_{JK}J(J+1)K^2-D_KK^4 \quad (1)$$

with the ground state constants held fixed. Due to the parallel nature of the transitions, $\Delta K=0$, and therefore only the upper state B, D_J, and D_{JK} molecular constants can be determined uniquely. Therefore, the upper state B,D_J,D_{JK} con-

TABLE II. Transition frequencies (cm^{-1}); $v_{HCl}=1\leftarrow 0$ a-type stretch excitation in $Ar_2H^{37}Cl$.

$J'_{K'_a,K'_c}\leftarrow J''_{K''_a,K''_c}$	Frequency $(o-c)$	$J'_{K'_a,K'_c}\leftarrow J''_{K''_a,K''_c}$	Frequency $(o-c)$	$J'_{K'_a,K'_c}\leftarrow J''_{K''_a,K''_c}$	Frequency $(o-c)$
$23_{0,23}\leftarrow 22_{0,22}$	2 881.870 76	$8_{6,3}\leftarrow 8_{4,4}$	2 880.836 76	$7_{0,7}\leftarrow 8_{0,8}$	2 880.181 51
$19_{0,19}\leftarrow 18_{0,18}$	2 881.677 17	$7_{4,3}\leftarrow 7_{4,4}$	2 880.830 94	$6_{2,5}\leftarrow 7_{2,6}$	2 880.181 51
$18_{0,18}\leftarrow 17_{0,17}$	2 881.628 13	$2_{0,2}\leftarrow 1_{0,1}$	2 880.799 40	$5_{2,3}\leftarrow 6_{2,4}$	2 880.181 51
$17_{0,17}\leftarrow 16_{0,16}$	2 881.578 88	$4_{2,2}\leftarrow 4_{2,3}$	2 880.789 15	$5_{4,2}\leftarrow 6_{4,3}$	2 880.131 69
$10_{8,3}\leftarrow 9_{8,2}$	2 881.568 21	$2_{2,1}\leftarrow 2_{0,2}$	2 880.751 32	$8_{0,8}\leftarrow 9_{0,9}$	2 880.123 62
$16_{0,16}\leftarrow 15_{0,15}$	2 881.528 92	$8_{6,2}\leftarrow 8_{6,3}$	2 880.728 00	$6_{4,3}\leftarrow 7_{4,4}$	2 880.067 46
$9_{6,3}\leftarrow 8_{6,2}$	2 881.504 46	$3_{2,1}\leftarrow 3_{2,2}$	2 880.728 00	$9_{0,9}\leftarrow 10_{0,10}$	2 880.065 62
$9_{8,1}\leftarrow 8_{8,0}$	2 881.498 42	$5_{4,1}\leftarrow 5_{4,2}$	2 880.704 70	$5_{4,1}\leftarrow 6_{4,2}$	2 880.061 60
$10_{6,5}\leftarrow 9_{6,4}$	2 881.489 02	$2_{2,0}\leftarrow 2_{2,1}$	2 880.681 69	$10_{0,10}\leftarrow 11_{0,11}$	2 880.007 37
$13_{0,13}\leftarrow 12_{0,12}$	2 881.377 81	$7_{6,1}\leftarrow 7_{6,2}$	2 880.677 58	$6_{4,2}\leftarrow 7_{4,3}$	2 879.994 71
$8_{4,4}\leftarrow 7_{4,3}$	2 881.337 59	$4_{4,0}\leftarrow 4_{4,1}$	2 880.669 86	$6_{6,0}\leftarrow 7_{6,1}$	2 879.974 57
$9_{4,6}\leftarrow 8_{4,5}$	2 881.331 40	$6_{6,0}\leftarrow 6_{6,1}$	2 880.661 10	$11_{0,11}\leftarrow 12_{0,12}$	2 879.948 83
$7_{4,3}\leftarrow 6_{4,2}$	2 881.292 27	$8_{8,0}\leftarrow 8_{8,1}$	2 880.656 39	$10_{2,9}\leftarrow 11_{2,10}$	2 879.948 83
$8_{4,5}\leftarrow 7_{4,4}$	2 881.279 55	$4_{4,1}\leftarrow 4_{4,0}$	2 880.646 20	$9_{2,7}\leftarrow 10_{2,8}$	2 879.948 83
$6_{4,2}\leftarrow 5_{4,1}$	2 881.232 01	$2_{2,1}\leftarrow 2_{2,0}$	2 880.638 12	$7_{4,3}\leftarrow 8_{4,4}$	2 879.944 62
$7_{2,5}\leftarrow 6_{2,4}$	2 881.174 34	$13_{12,1}\leftarrow 13_{12,2}$	2 880.629 68	$12_{0,12}\leftarrow 13_{0,13}$	2 879.890 02
$9_{0,9}\leftarrow 8_{0,8}$	2 881.171 44	$2_{0,2}\leftarrow 3_{0,3}$	2 880.465 74	$11_{2,10}\leftarrow 12_{2,11}$	2 879.890 02
$8_{0,8}\leftarrow 7_{0,7}$	2 881.119 23	$8_{4,4}\leftarrow 8_{6,3}$	2 880.443 50	$10_{2,8}\leftarrow 11_{2,9}$	2 879.890 02
$5_{2,3}\leftarrow 4_{2,2}$	2 881.071 84	$10_{6,4}\leftarrow 10_{8,3}$	2 880.419 05	$7_{6,1}\leftarrow 8_{6,2}$	2 879.846 76
$7_{0,7}\leftarrow 6_{0,6}$	2 881.066 49	$2_{2,1}\leftarrow 3_{2,2}$	2 880.416 76	$8_{6,3}\leftarrow 9_{6,4}$	2 879.839 12
$4_{2,2}\leftarrow 3_{2,1}$	2 881.021 56	$3_{0,3}\leftarrow 4_{0,4}$	2 880.409 55	$13_{0,13}\leftarrow 14_{0,14}$	2 879.830 71
$6_{0,6}\leftarrow 5_{0,5}$	2 881.013 37	$6_{2,5}\leftarrow 6_{2,4}$	2 880.401 25	$14_{0,14}\leftarrow 15_{0,15}$	2 879.771 19
$9_{4,6}\leftarrow 9_{2,7}$	2 881.001 09	$7_{2,5}\leftarrow 7_{4,4}$	2 880.397 29	$15_{0,15}\leftarrow 16_{0,16}$	2 879.771 54
$5_{0,5}\leftarrow 4_{0,4}$	2 880.959 99	$8_{4,5}\leftarrow 8_{4,4}$	2 880.394 35	$9_{8,2}\leftarrow 10_{8,3}$	2 879.703 19
$7_{2,5}\leftarrow 7_{2,6}$	2 880.954 53	$10_{6,5}\leftarrow 10_{6,4}$	2 880.387 48	$10_{8,3}\leftarrow 11_{8,4}$	2 879.613 59
$8_{4,5}\leftarrow 8_{2,6}$	2 880.949 02	$11_{6,5}\leftarrow 11_{8,4}$	2 880.373 90	$17_{0,17}\leftarrow 18_{0,18}$	2 879.591 31
$9_{4,5}\leftarrow 9_{4,6}$	2 880.941 25	$2_{2,0}\leftarrow 3_{2,1}$	2 880.365 79	$18_{0,18}\leftarrow 19_{0,19}$	2 879.530 56
$4_{0,4}\leftarrow 3_{0,3}$	2 880.906 29	$4_{0,4}\leftarrow 5_{0,5}$	2 880.353 28	$10_{8,2}\leftarrow 11_{8,3}$	2 879.524 95
$6_{2,4}\leftarrow 6_{2,5}$	2 880.901 40	$5_{0,5}\leftarrow 6_{0,6}$	2 880.295 97	$19_{0,19}\leftarrow 20_{0,20}$	2 879.469 69
$7_{4,4}\leftarrow 7_{2,5}$	2 881.896 38	$3_{2,1}\leftarrow 4_{2,2}$	2 880.288 77	$20_{0,20}\leftarrow 21_{0,21}$	2 879.480 21
$9_{6,4}\leftarrow 9_{4,5}$	2 881.883 01	$6_{0,6}\leftarrow 7_{0,7}$	2 880.238 83	$19_{2,18}\leftarrow 20_{2,19}$	2 879.408 21
$6_{4,3}\leftarrow 6_{2,4}$	2 881.841 57	$4_{2,2}\leftarrow 5_{2,3}$	2 880.234 25	$12_{10,3}\leftarrow 13_{10,4}$	2 879.394 32

stants are determined from a fit where ΔA and ΔD_K are fixed at zero, as listed in Table V. However, further information on ΔA and ΔD_K for the Ar_3HCl cluster can be obtained from least squares modelling of the Q-branch structure; these values are also reported in Table V. The final simulation using all the fitted parameters is presented in Fig. 2 and demonstrates that the shading and relative intensity of the Q-branch is well reproduced.

TABLE III. Spectroscopic constants (in cm^{-1}) determined from fits of the transition frequencies to an S-reduction Watson Hamiltonian using the III^r representation. The $v_{HCl}=0$ ground state values were fixed at values determined from microwave and far-IR studies.[a,b] The uncertainties in parentheses represent one standard deviation in the units of the last reported digit.

	$Ar_2H^{35}Cl$		$Ar_2H^{37}Cl$	
	$v_{HCl}=0$	$v_{HCl}=1$	$v_{HCl}=0$	$v_{HCl}=1$
A	0.0578 835 211(13)	0.057 841 7(16)	0.057 834 167(13)	0.057 859 02(33)
B	0.055 635 869(6)	0.055 050 8(17)	0.053 599 25(17)	0.053 027 7(43)
C	0.028 167 649(5)	0.028 018 08(37)	0.027 634 232(5)	0.027 485 11(57)
$D_J\times 10^5$	0.080 726(23)	0.080 15(37)	0.077 95(5)	0.085 8(18)
$D_{JK}\times 10^5$	−0.136 48(6)	−0.134 0(9)	−0.131 19(1)	−0.141 73(40)
$D_K\times 10^5$	0.062 306(47)	0.060 41(63)	0.059 47(13)	0.062 2(23)
$d_1\times 10^5$	−0.008 269(20)[c]	−0.008 91(40)	−0.009 763(3)[c]	−0.020 3(16)
$d_2\times 10^5$	−0.001 356(6)	−0.005 7(37)	−0.001 521(3)	−0.005(10)
v_0		2 882.751 76(3)		2 880.660 89(5)

[a]Reference 11.
[b]References 13–15.
[c]The d_1 values in Ref. 15 are reported as positive numbers; however, the near IR ground state combination differences unambiguously identify them to be negative numbers of the same magnitude. In the least squares fits, therefore, we use the more precise microwave/far-IR d_1 constants, but with the corrected sign.

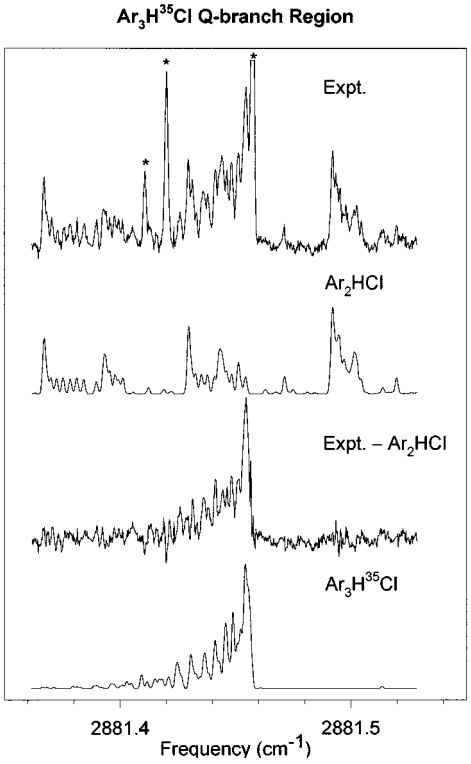

FIG. 2. Sample data indicating how Ar_3HCl and Ar_2HCl cluster spectra can be extracted separately. (a) The experimentally observed spectrum near the $Ar_3H^{35}Cl$ Q-branch region. (b) A least squares fit of the full Ar_2HCl spectrum in this region, which is a convolution of the calculated spectra for both the $Ar_2H^{35}Cl$ and $Ar_2H^{37}Cl$ complexes weighted by the 3:1 ^{35}Cl:^{37}Cl natural abundance ratio. (c) The contribution of just the Ar_3HCl clusters obtained by subtracting the Ar_2HCl model from the experimental spectrum [i.e., (a)–(b)]. (d) A least squares fit of the residual $Ar_3H^{35}Cl$ spectrum. The peaks marked with asterisks in (a) are due to contaminating ArHCl and $(HCl)_2$ species and have been subtracted in (b), (c), and (d).

TABLE IV. Transition frequencies (cm^{-1}) for the $v_{HCl}=1\leftarrow0$ parallel band of $Ar_3H^{35}Cl$.

$J'_{K'}\leftarrow J''_{K''}$	frequency $(o-c)$	$J'_{K'}\leftarrow J''_{K''}$	frequency $(o-c)$
$18_0 \leftarrow 17_0$	2 882.400 55(0)	$4_0 \leftarrow 5_0$	2 881.157 67(1)
$17_0 \leftarrow 16_0$	2 882.350 09(−2)	$5_0 \leftarrow 6_0$	2 881.099 92(1)
$16_0 \leftarrow 15_0$	2 882.299 47(−1)	$6_6 \leftarrow 7_6$	2 881.047 50(13)[b]
$15_9 \leftarrow 14_9$	2 882.259 49(17)[b]	$6_3 \leftarrow 7_3$	2 881.044 21(14)[b]
$15_6 \leftarrow 14_6$	2 882.252 67(1)	$6_0 \leftarrow 7_0$	2 881.041 32(−4)[b]
$15_0 \leftarrow 14_0$	2 882.248 49(0)	$7_6 \leftarrow 8_6$	2 880.987 84(0)
$14_6 \leftarrow 13_6$	2 882.201 27(0)	$7_0 \leftarrow 8_0$	2 880.983 48(2)
$14_0 \leftarrow 13_0$	2 882.197 12(1)	$8_6 \leftarrow 9_6$	2 880.928 88(−2)
$13_6 \leftarrow 12_6$	2 882.149 63(1)	$8_0 \leftarrow 9_0$	2 880.923 90(7)
$13_0 \leftarrow 12_0$	⋯[a]	$9_0 \leftarrow 10_0$	2 880.865 70(1)
$12_6 \leftarrow 11_6$	2 882.097 48(0)	$10_9 \leftarrow 11_9$	2 880.81 95(16)[b]
$12_0 \leftarrow 11_0$	2 882.093 24(1)	$10_0 \leftarrow 11_0$	2 880.806 64(3)
$11_0 \leftarrow 10_0$	2 882.040 75(0)	$11_6 \leftarrow 12_6$	2 880.751 31(1)
$10_6 \leftarrow 9_6$	2 881.992 33(1)	$11_0 \leftarrow 12_0$	2 880.745 39(−14)[b]
$10_0 \leftarrow 9_0$	2 881.988 22(3)	$12_9 \leftarrow 13_9$	2 880.698 07(13)[b]
$9_6 \leftarrow 8_6$	2 881.939 27(1)	$12_6 \leftarrow 13_6$	2 880.691 30(0)
$9_0 \leftarrow 8_0$	2 881.935 03(2)	$12_0 \leftarrow 13_0$	2 880.686 32(−6)
$8_0 \leftarrow 7_0$	2 881.881 10(−2)	$13_0 \leftarrow 14_0$	2 880.626 59(−2)
$7_0 \leftarrow 6_0$	2 881.827 77(3)	$14_6 \leftarrow 15_6$	2 880.570 68(1)
$6_0 \leftarrow 5_0$	⋯[a]	$14_0 \leftarrow 15_0$	2 880.566 29(0)
$5_0 \leftarrow 4_0$	2 881.718 77(−2)	$15_9 \leftarrow 16_9$	2 880.514 87(−3)
		$15_6 \leftarrow 16_6$	2 880.509 61(−2)
		$15_0 \leftarrow 16_0$	2 880.505 65(1)
		$16_6 \leftarrow 17_6$	2 880.448 91(2)
		$16_0 \leftarrow 17_0$	2 880.443 50(−10)[b]
		$17_6 \leftarrow 18_6$	2 880.387 49(2)
		$17_0 \leftarrow 18_0$	2 880.383 15(0)
		$18_6 \leftarrow 19_6$	2 880.325 85(3)
		$18_0 \leftarrow 19_0$	⋯[a]

[a]Peaks obscured by strong overlapping Ar_2HCl, ArHCl, or HCl_2 lines.
[b]Peaks are blended with Ar_2HCl transitions, and not used in the least squares fit.

Further corroboration of the above $Ar_3H^{35}Cl$ assignment is substantiated by identifying the corresponding $Ar_3H^{37}Cl$ band. Based on the observed S/N ratio of 10 on the $Ar_3H^{35}Cl$ Q-branch, the corresponding Q-branch feature for $Ar_3H^{37}Cl$ is expected approximately 2 cm^{-1} to the red with a S/N~3. Indeed, a Q-branch with the correct relative intensity at 2.1 cm^{-1} to the red of the feature assigned to $Ar_3H^{35}Cl$ is observed. However, since the associated P/R-branch transitions are resolved and therefore weaker still, a complete assignment of the corresponding $Ar_3H^{37}Cl$ spectrum has not been attempted.

IV. DISCUSSION

The data obtained for Ar_2HCl and Ar_3HCl in the infrared region of the spectrum allow us to pursue an analysis of the vibrationally averaged geometries in the $v_{HCl}=1$ manifold. However, the use of a geometric analysis need not imply a ''rigid'' structure; indeed, large amplitude motion of the HCl subunit is clearly indicated by the data. From the structural analysis of Ar_2HCl there are indications already that nonpairwise additive forces are significant. The vibrational redshifts for Ar_nHCl $(n=1-3)$ clusters display much more of a linear dependence on n than in the analogous Ar_nHF complexes. Insight into these differences is provided by analysis of the Ar–HCl and Ar–HF pair potentials. Finally, theoretical investigation of the equilibrium structures and vibrational redshifts for larger clusters are performed to examine the size dependence.

TABLE V. Spectroscopic constants (in cm^{-1}) determined from fits of the transition frequencies to a symmetric top Hamiltonian. The $v_{HCl}=0$ ground state values were fixed at values determined from microwave transitions. The uncertainties in parentheses represent one standard deviation in the units of the last reported digit.

	$Ar_3H^{35}Cl$	
	$v_{HCl}=0$	$v_{HCl}=1$
B	0.028 149 387(3)	0.027 997(2)
$D_J\times10^8$	7.782(7)	8.59(59)
$D_{JK}\times10^8$	6.064(20)	10.12(28)
$\Delta(A-B)\times10^4$	1.41(6)[a]	
$\Delta D_K\times10^8$	4.0(35)[a]	
v_0	2 881.442 17(2)	

[a]Due to the parallel nature of this band, only differences can be determined.

A. Vibrationally averaged structures

The infrared cluster spectra for Ar_nHCl ($n=1,2,3$) contain structural information on the ground and vibrationally excited states through the rotational constants, which are inversely proportional to the corresponding moments of inertia. The resulting structures necessarily represent vibrationally averaged geometries, and as a consequence of large amplitude motion of the HCl subunit, can differ substantially from the equilibrium structures. This makes unambiguous interpretation of structural parameters more difficult, since for increasing number of Ar atoms there are far more large amplitude coordinates than rotational constants. Nevertheless, by fixing some of the more ''rigid'' internal degrees of freedom, vibrationally averaged structural parameters (based on an explicit model) can be extracted which prove instructive in probing intermolecular forces in these multibody systems.

The effect of HCl excitation on the Ar_nHCl vibrationally averaged geometry can be determined from a comparison of the rotational constants in the ground and excited vibrational states. There are extensive microwave,[27–29] far-,[30–35] and near-infrared[25,36] spectroscopic measurements on ArHCl; a brief description of some of the changes in the vibrationally averaged ArHCl structure between the $v_{HCl}=0$ and $v_{HCl}=1$ vibrational manifolds is illustrative of trends observed in the higher Ar_nHCl clusters. In ArHCl there is a 0.93% decrease in the B value corresponding in a pseudodiatomic approximation to a 0.47% increase (0.0186 Å) in R_{eff}, the distance between the HCl center-of-mass (com) and the Ar atom. This is somewhat unusual, since the monomer vibrational frequency red-shifts by 1.7667 cm^{-1} upon complexation with a single Ar atom, indicating a slight increase in the well depth in the $v_{HCl}=1$ state. Indeed, much of this shift toward larger R_{eff} values in the $v_{HCl}=1$ state can be accounted for by the anharmonic stretching of the HCl bond with one quantum of vibrational excitation which pushes the Ar out due to repulsive interactions with the hydrogen atom. Based on these results for ArHCl, one would therefore predict the analogous rotational constants in the larger Ar_nHCl clusters also to decrease due to a comparable increase in the Ar_n–HCl com separation.

A full inertial analysis of the actual equilibrium structure of Ar_2HCl necessarily must include vibrational averaging over large amplitude motion and requires information not contained in the three near-IR rotational constants. Consequently, we invoke a more simplified approach, in which contributions from large amplitude motion are absorbed into the rotational constants A, B, and C, which are then used to determine effective, vibrationally averaged center-of-mass separations between Ar–Ar (ρ_{eff}) and Ar_2–HCl (R_{eff}). This requires an explicit model for the vibrationally averaged geometry of the cluster, which we take to be planar with the HCl pointing along the C_{2v} axis. This leads to the simple analytical expressions for R_{eff} and ρ_{eff},

$$R_{eff}=\sqrt{(P_A+I_{HCl})/\mu}, \tag{2a}$$

$$\rho_{eff}=\sqrt{(2P_B/m_{Ar})}, \tag{2b}$$

where P_A and P_B are the planar moments [e.g., $P_A=1/2(-I_A+I_B+I_C)$], I_{HCl} is the HCl moment of inertia, μ is the Ar_n–HCl reduced mass, and m_{Ar} is the Ar mass. With these simple expressions we can attempt to interpret the small shifts both upon complexation and vibrational excitation of the monomer.

In the ground vibrational state, Eq. (2a) leads to $R_{eff}=3.4969$ and 3.4975 Å for $Ar_2H^{35}Cl$ and $Ar_2H^{37}Cl$, respectively. The fact that the center of mass separation is smaller for the ^{35}Cl isotope is consistent with the HCl oriented with the hydrogen atom pointing toward the Ar_2 com. For the $v_{HCl}=1$ vibrational state, R_{eff} increases by 0.0186 Å to 3.5155 and 3.5165 Å for $Ar_2H^{35}Cl$ and $Ar_2H^{37}Cl$, respectively. This is in essentially perfect agreement with the shift in R_{eff} observed for ArHCl upon vibrational excitation of the HCl subunit. A somewhat different trend is seen in the vibrationally averaged Ar–Ar distance. In the ground state, $\rho_{eff}=3.8323$ Å for $Ar_2H^{35}Cl$, whereas in the excited state this value is essentially unchanged, i.e., $\rho_{eff}=3.8324$ Å. Thus, vibrational excitation of the HCl would appear to have almost no effect on the vibrationally averaged Ar–Ar separation, a trend which is echoed in both isotopes. This is at first glance quite surprising, since both the experimentally measured red-shifts of the Ar_nHCl clusters as well as the pairwise Ar–HCl potentials would predict a stronger attraction of each Ar atom to the HCl monomer upon vibrational excitation. This should ''squeeze'' the two Ar atoms closer together, and cause ρ_{eff} to decrease slightly. However, the triangular equilibrium geometry of the Ar_2HCl complex is at the optimum geometry for both Axilrod–Teller (triple dipole[37,38]) and induced dipole-induced dipole repulsive three-body interactions, which would tend to increase the Ar–Ar separation. For Ar_2HCl, the competition between pairwise additive squeezing and repulsive three-body effects fortuitously cancel, which leads to essentially no change in Ar–Ar distance upon HCl vibrational excitation.

Further evidence in support of this interpretation can be found by comparison with the vibrationally averaged Ar–Ar separation in the bare Ar_2 dimer, in which all three-body effects are obviously absent. For the Ar_2 dimer,[39,40] $\rho_{eff}=3.821(10)$ Å i.e., a considerable 0.011 Å shorter than in the Ar_2HCl trimer cluster. A similar estimate for the magnitude of these three-body effects on the Ar–Ar separation in Ar_2HCl can be made using the theoretical rotational constants reported by Cooper and Hutson,[21] calculated using both (i) the pairwise additive potential and (ii) the pairwise additive potential modified with three-body terms due to Axilrod–Teller, induced dipole-induced dipole, and exchange quadrupole effects. Based on the vibrationally averaged inertial analysis embodied in Eq. (2), ρ_{eff} is predicted to increase by 0.028 Å from 3.810 to 3.838 Å when such three-body terms are included. Thus, the experimentally observed increase in ρ_{eff} from Ar_2 to Ar_2HCl, as well as the subsequent insensitivity of ρ_{eff} to HCl vibrational excitation is qualitatively consistent with modeling by Cooper and Hutson of three-body forces in Ar_2HCl.

Finally, we return briefly to the issue of vibrational av-

eraging effects by examining the inertial defect, $\Delta=(I_C-I_A-I_B)$, which should vanish for a rigid planar structure. Furthermore, positive or negative values of the inertial defect reflect the degree of in-plane vs out-of-plane large amplitude motion around a nominally planar geometry. The inertial defect in the $v_{\mathrm{HCl}}=1$ state for $Ar_2H^{35}Cl$ is relatively large and positive ($\Delta=4.006$ amu Å^2), which would be consistent with significant in-plane zero-point vibrational motion of either the Ar_2 or HCl subunits. A positive contribution to the inertial defect by in-plane zero-point motion of the light H atom would be consistent with the ''softer'' in-plane (37.195 cm^{-1}) vs out-of-plane (45.203 cm^{-1}) intermolecular frequencies measured in the ground HCl vibrational state.[13,14] However, this H atom motion is not likely to be the dominant contribution, since the inertial defect is also positive even in the out-of-plane intermolecular excited state. This suggests that the inertial defect is dominated by in-plane zero-point motion of the heavy atom species, i.e., either the van der Waals stretch or bending/stretching motion of the Ar_2 subunit. Similar trends have been noted in near-IR combination band studies of intermolecular modes in Ar_2HF and Ar_2DF clusters as well.[17]

The Ar_3HCl spectrum reflects parallel band excitation of a symmetric top, and as a result, there is a limited number of spectroscopic parameters from which to determine vibrationally averaged structural data. Furthermore, there are several additional torsional and bending vibrations of the Ar_3 subunit which may further complicate the influence of vibrational averaging on the rotational constants. Nevertheless, if we model Ar_3–HCl as a pseudodiatomic with the Ar_3 plane perpendicular to a C_{3v} Ar_3–HCl axis, then we can solve for the vibrationally averaged separation between the com of Ar_3 and HCl subunits from the B rotational constant. From the values in Table V, one calculates that R_{eff} increases by +0.54% from 3.299 Å in the ground vibrational state to 3.317 Å in the $v_{\mathrm{HCl}}=1$ excited state, i.e., increasing consistently by the same 0.018 Å that is observed in both Ar–HCl and Ar_2–HCl complexes. Similar quantitative data on the change in the Ar–Ar distance ρ_{eff} are not easily available, since there is no information in a parallel band on the A rotational constant. However, the spectra do constrain $\Delta(A-B)$, which, with the experimentally measured value of ΔB, determines ΔA to be quite small $[-1.1(6)\times10^{-5}$ cm$^{-1}]$. Based on theoretical predictions of $C=0.029\,07$ cm^{-1} for the Ar_3 trimer, this would imply that ρ_{eff} in Ar_3–HCl does not change by more than a few parts in 10^4 upon vibrational excitation. This again would be consistent with the comparable insensitivity to HCl monomer vibrational excitation observed in both Ar_2HCl isotopomers, and attributed previously to a delicate balance between (i) squeezing of the Ar–Ar bonds due to site competition for the HCl and (ii) increased three-body Ar_3 repulsion in the vibrationally excited state.

B. Predicted Ar_nHCl equilibrium structures

In the Ar_nHF and Ar_nDF series, pairwise additive potentials constructed from the well studied Ar–HF and Ar–Ar potentials proved quite useful in characterizing the equilibrium structures of the various cluster sizes. Similarly, we have constructed pairwise additive potentials for Ar_nHCl based on (i) the H6(4,3,0) ArHCl potential of Hutson[3] and (ii) the Ar–Ar potential of Aziz *et al.*,[41] which allows the equilibrium structure and binding energy for clusters to be calculated as a function of n. Specifically, we use the approximate pairwise additive potential for Ar_nHCl combined with a quasi-Newton algorithm to search for local and global minima on the full potential surface. In the following section we restrict the discussion to relatively small clusters ($n\leqslant4$) representative of the range experimentally observed. However, later we will return to predictions for much larger clusters more characteristic of the bulk matrix phase.

The lowest energy structures for $n=1,2,3$ are qualitatively identical to the structures determined for Ar_nHF. The symmetries of equilibrium structures of Ar_2HCl (C_{2v}) and Ar_3HCl (C_{3v}) are also consistent with the number of equivalent Ar atoms determined from the nuclear spin statistics present in spectra of these clusters. For Ar_nHCl ($n=1,2,3$) the next higher minima are calculated to be 28, 57, and 133 cm^{-1} higher in energy. For both ArHCl and Ar_2HCl the next higher energy ''isomer'' is obtained by a rotation of the HCl monomer by 180° to form the ArClH and Ar_2ClH structures, respectively. Experimental information on these ''isomers'' has been obtained by infrared excitation of the Σ bend in ArHCl (23.6572 cm^{-1}) and in Ar_2HCl (39.5547 cm^{-1}). The predictive power of such a simple classical analysis is encouraging and suggests it is worth while to pursue the same approach to predict the structures of still larger Ar_nHCl clusters.

The global minimum for Ar_4HCl is a structure with C_{2v} symmetry with a binding energy of -1087.9 cm^{-1}. The next higher minimum (C_{3v}) is only 19.0 cm^{-1} higher in energy, but the two minima are separated by a barrier of approximately 100 cm^{-1}. This is qualitatively different than both predicted and observed in Ar_4HF, where the C_{3v} isomer appears to be the true global minimum and the C_{2v} isomer minimum is theoretically predicted to be 15.43 cm^{-1} higher in energy.[42] Interestingly, we have not been able to observe the corresponding C_{3v} $n=4$ cluster spectrum in Ar_nHCl, even though we currently detect the Ar_3HCl cluster with even higher S/N than in the previous Ar_3HF studies. If the C_{2v} structure in fact survives as the global minimum after zero-point effects are included, this may partially be due to a lack of a strongly overlapped Q-branch predicted for the perfectly symmetric C_{3v} structure, which for low concentrations presents a far more readily sharp feature in a congested spectrum. Such differences between Ar_4HCl and Ar_4HF underscore the subtle balance of forces that takes place in finite size clusters, whereby small changes in the pairwise interactions can be responsible for shifts in the energy ordering of isomers, and thus influence the predominant structures of clusters observed under supersonic jet conditions.

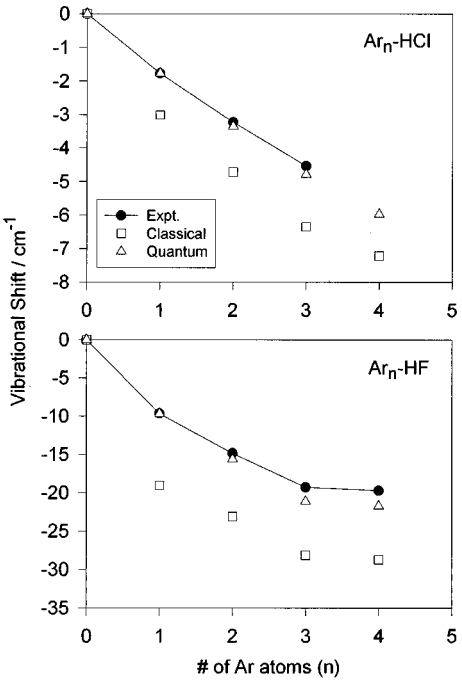

FIG. 3. The experimental HX vibrational shifts for (upper) Ar_nHCl and (lower) Ar_nHF as a function of n. Also included are the calculated shifts from (i) classical calculations and (ii) quantum variational and Monte Carlo calculations (Refs. 24,46,47).

C. Vibrational red-shifts

Another window into the size-dependent effects of sequential solvation of HCl in Ar afforded by near infrared studies is the red-shift of the high frequency HCl stretch upon complex formation. As in Ar_nHF/DF there exists a rigorous methodology for calculating the size dependence of the HCl vibrational red-shift in the Ar_nHCl system. Specifically, by taking advantage of the well known Ar–HCl and Ar–Ar pair potentials, the intermolecular wave functions can be rigorously calculated on both the $v_{HCl}=0$ and $v_{HCl}=1$ adiabatic potentials; the difference in the ground state energies on these two potentials is equal to the red-shift induced by complexation. There are only two approximations in this procedure, (i) the adiabatic separability of the high frequency HCl stretch vibration from the low frequency intermolecular motion, and (ii) the assumption of perfect pairwise additivity in the potential surface. The first approximation has proven to be quite valid in both ArHF and ArHCl; consequently, the magnitude of the second pairwise additive approximation can be tested by comparison with experiment. The experimental red-shifts are plotted in Fig. 3, for both Ar_nHCl and Ar_nHF, and the Ar_nHCl values are reported in Table VI.

In order to obtain some preliminary information about the size dependence of the HCl vibrational red-shifts in Ar_nHCl clusters based on the pairwise additive potential, we resort to a simple approximation where the red-shift in Ar_nHCl is modeled by the change in the absolute well depth (D_e) of the potential caused by vibrational excitation of the HCl from $v_{HCl}=0$ to $v_{HCl}=1$. Though purely classical, this method has the advantage of simplicity, can be applied to arbitrarily sized clusters, and therefore provides useful qualitative insight into the relationship between HCl vibrational red-shift and the size/geometry of the complex. As we will later show, it also permits intriguing contrast with similar classical studies of larger Ar_n–HF clusters by Bacic *et al.*[43]

TABLE VI. Experimental HCl vibrational origins and the corresponding red-shifts for Ar_nHCl ($n=1-4$) clusters. Included are red-shifts calculated using the approximate classical method and variational[a] ($n=1$) and Quantum Monte Carlo[b] ($n=2-4$) techniques. The experimental matrix shift[c] is also included for comparison.

	Origin	Red-shift	Classical	Quantum
HCl	2 885.975 4			
ArHCl	2 884.208 7	−1.766 7	−3.012	−1.765[a]
Ar_2HCl	2 882.751 8	−3.223 6	−4.717	−3.35(7)[b]
Ar_3HCl	2 881.442 2	−4.533 2	−6.343	−4.78(7)[b]
Ar_4HCl	···	···	−7.215	−5.97(14)[b]
Ar matrix	2 870.80[c]	−15.18		

[a]Reference 3.
[b]Reference 24.
[c]Reference 22.

As seen in Fig. 3, such classical calculations for HF/HCl vibrational red-shifts do not quantitatively reproduce the high resolution experimental results. Specifically, these calculations (see Fig. 3) consistently overestimate the red-shift for $n=1-4$ clusters, by an amount which is nearly constant at $\approx 9-11$ cm^{-1} and $\approx 1.5-2.0$ cm^{-1} for HF and HCl clusters, respectively. Conversely, 5D quantum variational[42,44,45] and/or full diffusion quantum Monte Carlo[46,47] calculations have been performed for the Ar_nHF clusters (see Fig. 3), which are in nearly quantitative agreement with experiment. The source of this much larger shift between classical and quantum predictions is readily interpreted in terms of a HF vibrational dependence to intermolecular zero-point energy, which must therefore increase by $\approx 9-11$ cm^{-1} in the $v_{HF}=1$ state. This hypothesis can of course be explicitly verified for the $n=1$ ArHF cluster where all intermolecular vibrations have been spectroscopically observed, and quantum calculations on the H(6,3,2) potential indicate a ≈ 9.4 cm^{-1} increase in zero-point energy between $v_{HF}=0$ and $v_{HF}=1$ intramolecular excitation. Somewhat more surprising is that this increase in zero-point energy appears to be relatively insensitive to the number of Ar atoms from $n=1$ to 4. However, this would be consistent with a simple picture that these shifts are dominated by HX bending and Ar_n–HX van der Waals stretch modes. From a similar line of argument, the consistent overestimation of redshifts in the corresponding Ar_nHCl complexes indicate that the zero-point energy increases by a more modest $\approx 1.5-2.0$ cm^{-1} in the $v_{HCl}=1$ state.

The availability of vibrational red-shift data on both Ar_nHCl and Ar_nHF clusters permit a direct comparison of ''solvation'' effects in these two systems. First of all, both series of complexes display a monotonic increase in the red-shift as Ar atoms are added sequentially. This largely reflects the vibrational state dependent change in the corresponding dimer potentials. Specifically, the binding energies in the $v_{HX}=1$ vs $v_{HX}=0$ state increase by 3.0 cm^{-1} and

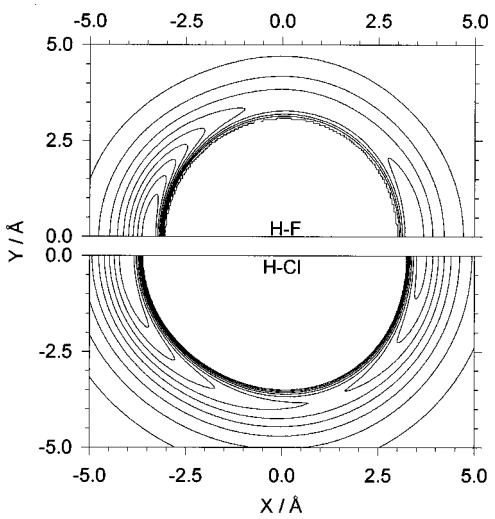

FIG. 4. Contour plots of the H6(4,3,2) Ar–HF (upper) and H6(4,3,0) Ar–HCl (lower) intermolecular potentials in Cartesian coordinates (Å) with the HX center-of-mass placed at the origin and the H-atom pointing in the negative x-direction. In each plot there are 10 equally spaced contours indicating the bound ($E \leqslant 0\ \mathrm{cm}^{-1}$) region of the potential. Notice that the global minimum of the Ar–HF potential is at a smaller distance from the origin and the greater angular anisotropy of the Ar–HF potential.

19.0 cm^{-1}, respectively, for Ar–HCl and Ar–HF, thus redshifting the HX vibrational frequency upon complex formation. As predicted from a simple pairwise additive model, this redshift monotonically increases with number of Ar atoms, though the magnitude of these incremental red-shifts is clearly sensitive to (i) differences in the v_{HX}-dependent Ar–HF vs Ar–HCl pair potentials, (ii) the vibrationally averaged locations of the additional Ar atoms, as well as (iii) more subtle nonpairwise additive interactions.

The different incremental red-shifts for Ar_nHCl and Ar_nHF can be understood from an examination of the two Ar–HX pair potentials. In the case of Ar_n–HF, the first Ar produces by far the largest incremental red-shift ($\approx 10\ \mathrm{cm}^{-1}$), with progressively weaker red-shifts for additional Ar atoms. By way of contrast, the red-shift for the first Ar atom in Ar–HCl is much smaller ($\approx 2\ \mathrm{cm}^{-1}$) and much more nearly constant per additional atom. The incremental red-shift behavior in Ar–HF has been explained as due to a combination of angular ''competition'' of the Ar atoms for the linear global minimum geometry, and the significant angular anisotropy of Ar–HF $v_{\mathrm{HX}}=1$ and 0 potentials. This differs qualitatively from the nearly linear redshifts observed and predicted in $\mathrm{Ar}_n\mathrm{CO}_2$, where there are multiple nearly isoenergetic T-shaped binding sites for the initial several Ar atoms.[48] Examination of the Ar–HF and Ar–HCl potentials in Fig. 4 illustrates qualitatively why the Ar_nHCl incremental red-shift is nearly constant. First of all, the angular anisotropy of the Ar–HCl potential is significantly less ''focused'' at the linear configuration than is the case for Ar–HF. Secondly, the Ar–HCl potential minima occur at larger values of R than for Ar–HF, so that more than one Ar atom can sample the HCl well region without being energetically penalized by strong Ar–Ar repulsion. This combination of effects make the binding of successive Ar atoms to HCl much more ''equivalent'' than for Ar_nHF and thus resulting in a more linear dependence of the red-shift on n.

Finally, we can eliminate the zero-point contributions to the red-shift for small clusters of Ar_nHCl by comparison with diffusion Quantum Monte Carlo calculations by Lewerenz.[24] These calculations are based on the same pairwise additive potential surfaces used in the classical calculations; the ground state energy differences obtained for clusters with $v_{\mathrm{HCl}}=1$ and 0 correspond to the pairwise additive redshifts predicted in the corresponding cluster. The results, shown in Fig. 3 and included in Table VI, indicate a greatly improved but still not perfect agreement with the experimental red-shifts. In particular, the predicted redshifts for the trimer and tetramer are larger by $\approx 5\%$ than experimentally observed, which is consistent with similar trends observed in Ar_nHF and Ar_nDF clusters. Based on the quantitative success of the Ar–HCl surface in reproducing high resolution near and far-IR spectroscopic observations, the residual discrepancies are therefore almost certainly due to neglect of three-body interactions in the pairwise additive surface and, as in Ar_nHF/DF clusters, may be used for further rigorous tests of non-pairwise additive force models.

D. Extrapolation to matrix isolation studies

An implicit goal in the study of finite size clusters is to obtain sufficiently accurate multidimensional intermolecular potentials (both pairwise and nonpairwise) in order to permit realistic predictive models of condensed phase behavior to be constructed. Specifically, the present work provides a direct connection with bulk phase FTIR studies of HCl in cryogenic Ar matrices.[22,23] Though the level of detail provided by such matrix isolation studies is limited by lower resolution in the condensed phase, comparisons can nevertheless be made at the level of HCl vibrational redshifts as a function of the surrounding Ar environment. With this goal in mind, we have used the simple pairwise additive Ar_nHCl potential discussed in Sec. IV B to obtain minimum energy structures for $n \leqslant 54$ Ar atoms. Furthermore, since the Ar–HCl potential is parameterized as a function of v_{HCl}, the vibrational red-shift for this structure can be estimated from the $v_{\mathrm{HCl}}=1 \leftarrow 0$ energy difference for a given minimum energy structure for a given number of Ar atoms. Though the simplicity of this classical model neglects zero-point motion as well as three-body (and higher order) interactions among the subunits, it does offer the corresponding advantage of consistency of method for clusters large enough to approximate behavior under bulk conditions. Specifically, the results reported here correspond to up to 4 ''solvent shells'' ($n \leqslant 54$), which, though not impossible to model theoretically with diffusion Quantum Monte Carlo methods, would make rigorous calculations of the redshifts and vibrationally averaged structures exceedingly difficult.

This question is addressed as follows. Computational studies of Ar_nHCl with $n=1-12$ have been performed to establish trends in the equilibrium structures near the global minima for each cluster size (see Fig. 5). Interestingly,

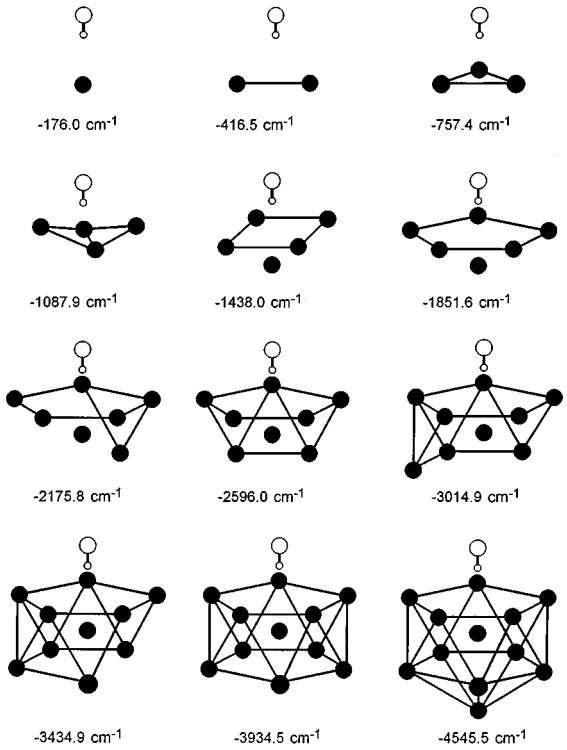

FIG. 5. Pictorial representations of the minimum energy structures for the Ar_nHCl ($n=1-12$) series. The numbers under each structure are the binding energies in cm^{-1}.

though $n=12$ corresponds to the first shell occupancy for an octahedral site in a fcc matrix, this does not necessarily imply that the lowest energy structure is HCl fully solvated by Ar atoms. Indeed, for Ar_nHCl clusters from $n=1$ to 12, the lowest energy structural motif reflects build up of a solvation ''cap'' localized around the H-atom end of HCl. Though

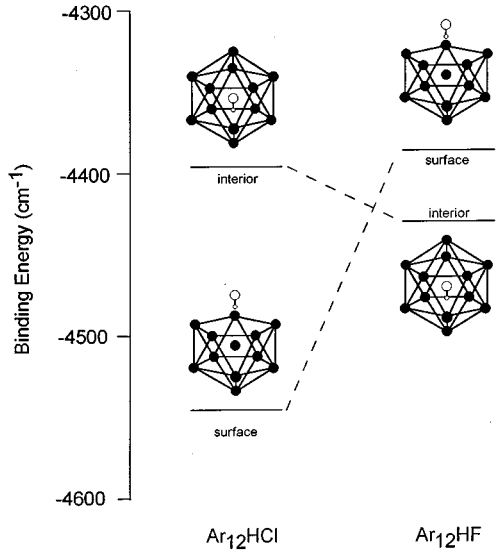

FIG. 6. Plot of the calculated binding energies for surface and interior HX(X=Cl, F) sites in an Ar_{12} cluster. Note that the HCl prefers a surface site while the HF adopts a fully solvated geometry.

there are numerous higher-lying local minima for the larger clusters, the structures in Fig. 5 reflect global minima, which do not require significant reorganization of the first shell from Ar_nHCl to $Ar_{n+1}HCl$. Of course, there are also local minima corresponding to ''fully solvated'' cluster geometries for $n\approx12$, but the model predicts these to be $\approx149\ cm^{-1}$ *higher* than the energetically more stable ''partially solvated'' geometries. The key point of these results is that the pairwise additive potentials predict that HCl prefers to form ''surface'' vs ''interior'' sites in a finite size Ar cluster.

It is worth noting that this is qualitatively different from the behavior previously found by Bacic *et al.* in $Ar_{12}HF$ clusters,[43] where the fully solvated geometry is $>40\ cm^{-1}$ *lower* in energy than any partially solvated isomeric geometries. This is clearly demonstrated in Fig. 6, which indicates the local structural minima and corresponding energies for both interior and surface adsorbed HCl and HF in an Ar_{12} cluster. This is not due simply to a competition between the energetics of the two pairwise binding potentials, which are relatively close ($D_e=-220.2\ cm^{-1}$ and $-176.0\ cm^{-1}$ for ArHF and ArHCl) and both substantially in excess of the Ar–Ar binding energy ($D_e=99.5\ cm^{-1}$). What appears to be more important is the larger van der Waals ''size'' of the HCl vs HF in the matrix (i.e., see Fig. 4), and thus the significant distortion of the Ar matrix upon substitution of a HCl vs HF subunit. In essence, the HCl molecule is too big to be solvated in the middle of the Ar_{12} cluster; instead, the energetically more favorable configuration is with the HCl on the surface where the Ar atoms can adopt the bare Ar_{12} minimum energy structure. This emphasizes the delicate balance between the Ar–Ar and Ar–HCl intermolecular forces present in these clusters. In addition, it highlights the difficulty in extrapolating structural results for small clusters, which are dominated by Ar–HCl interactions, to the bulk where structure is dominated by the many Ar–Ar interactions.

In a typical experimental preparation of an Ar/HCl matrix, the HCl is trapped in an interior site by coadsorption of the Ar/HCl gas mixture and which for an annealed Ar crystal would correspond to a single substitution site in a fcc lattice. Consequently, in order to best compare red-shifts predicted from the Ar_nHCl pairwise additive potential with those of the matrix, local energetic minima for finite Ar_nHCl clusters have been obtained as a function of the number of solvation shells, n_{shell}. In order to best approximate the matrix structure for finite n_{shell}, the minimization procedure is started with the HCl molecule substituted for a single Ar atom symmetrically in the center of a perfect fcc lattice. Local minimization of the first fcc solvation shell ($n_{\text{Ar}}=12$) collapses to the icosahedral structure discussed previously, but this is still higher in energy than the ''surface site'' HCl. Also worth noting is that this slight energetic preference for an icosohedral vs fcc lattice structure at the first solvation shell level is quickly shifted with additional solvent shells. For $n_{\text{Ar}}=18$, the six additional nearest neighbors ''squeeze'' the first solvation shell to form a minimum energy structure that is much closer to a perfect fcc lattice. Though it is always

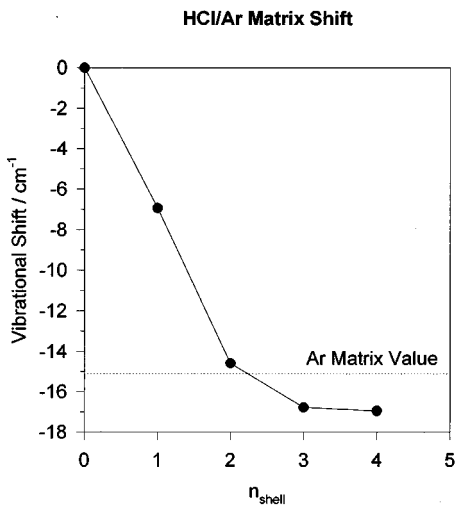

FIG. 7. Calculated HCl vibrational shift as a function of the number of fcc solvation shells. The dashed line indicates the experimental Ar matrix value.

difficult to identify a given structure unambiguously as a global vs local energetic minimum on such a multidimensional potential, all structures determined from different starting structures (e.g., icosahedral) result in higher energy structures. Energy minimization for the next two solvation shell structures ($n_{\mathrm{Ar}}=42$ and $n_{\mathrm{Ar}}=54$) starting from a perfect fcc lattice serves to stabilize this incipient fcc structure further into place, as indeed expected in the limit of the bulk matrix. It is important to note that these structures are fully relaxed, and to the best of our knowledge represent the unstrained, local minimum energies for HCl surrounded by a specific number of solvation shells.

With the procedure reasonably converged for obtaining the local fcc lattice structures around the HCl subunit, it makes sense to look at the vibrational red-shifts as a function of solvation shell number. The results for the first four solvation shells are reported in Fig. 7, and indicate several interesting points. First of all, the HCl vibrational red-shift for the first solvent shell is $\approx 6.9\ \mathrm{cm}^{-1}$, which is less than half of the $15.18\ \mathrm{cm}^{-1}$ red-shift observed in matrix isolation studies. This is qualitatively different from what had been previously noted in similar theoretical studies of $\mathrm{Ar}_n\mathrm{HF}$ clusters,[43] where the first solvent shell had already achieved a red-shift ($44.70\ \mathrm{cm}^{-1}$) within 10% of the experimental matrix results. As a necessary corollary, the red-shifts predicted for HCl continue to grow significantly beyond the first solvation shell, reaching an asymptotic value only after closure of the third or fourth shell. Stated in simple physical terms, the HCl chromophore ''feels'' the environment of the Ar lattice well beyond its nearest neighbors, in clear contrast to the behavior inferred for HF in matrices. Of course, this effect must eventually saturate with the number of solvation shells; by $n_{\mathrm{shell}}=4$, the predicted red-shift of $\approx 17\ \mathrm{cm}^{-1}$ for $\mathrm{Ar}_n\mathrm{HCl}$ is in qualitatively good agreement with the experimental matrix result of $15.18\ \mathrm{cm}^{-1}$.

More quantitatively, however, the results of these classical red-shift calculations for sequential solvation of HCl by Ar clearly overshoot the matrix value by $\approx 1.8\ \mathrm{cm}^{-1}$. Though only 10% of the total red-shift, this discrepancy is quite similar to the trend established for small $\mathrm{Ar}_n\mathrm{HCl}$ ($n=1,2,3$) clusters, which also overestimate the experimental red-shifts by $\approx 1.5\ \mathrm{cm}^{-1}$. From comparison of predicted with experimental red-shifts in Fig. 3, these appear to be a nearly constant offset for both HCl and HF clusters and due predominantly to neglect of zeropoint motion and three-body interactions in these calculations. Indeed, if we take the red-shift discrepancy for the largest cluster ($n=3$) as an approximate measure of this error, the corrected prediction for the HCl red-shift in an Ar matrix would be $\approx 15.2\ \mathrm{cm}^{-1}$, i.e., in essentially quantitative agreement with the $15.18\ \mathrm{cm}^{-1}$ experimental result.

V. SUMMARY

High-resolution, rotationally resolved spectra of the $v_{\mathrm{HCl}}=1\leftarrow 0$ stretch in $\mathrm{Ar}_2\mathrm{HCl}$ and $\mathrm{Ar}_3\mathrm{HCl}$ have been recorded using a slit-jet infrared spectrometer. For both clusters the Ar atoms are distributed symmetrically about the HCl axis, on the H-atom side of the HCl. Near-infrared excitation of the $\mathrm{Ar}_n\mathrm{HCl}$ complexes slightly increases the vibrationally averaged $\mathrm{Ar}_n-\mathrm{HCl}$ center-of-mass separation, but the magnitude of these changes is insignificant compared with the large amplitude motion present in these clusters. Structural analysis of the $\mathrm{Ar}_2\mathrm{HCl}$ trimer does show evidence for nonpairwise intermolecular forces, and the magnitude of structural changes are consistent with previous theoretical work on three-body repulsion in $\mathrm{Ar}_n\mathrm{HCl}$. At least for the complexes studied experimentally, the sequential growth of Ar around the HCl chromophore is identical to the analogous $\mathrm{Ar}_n\mathrm{HF}$ ($n=1-3$) complexes due to the similarities in the Ar–HX potentials.

The vibrational frequency of HCl monotonically shifts to the red with sequential addition of Ar atoms but does not display the strong nonlinearity measured in $\mathrm{Ar}_n\mathrm{HF}$ ($n=1-4$). This difference in the behavior of the sequential red-shift reflects the less anisotropic nature of the angular-radial Ar–HCl potential. Quantum calculations of the vibrational red-shift in the $\mathrm{Ar}_n\mathrm{HCl}$ clusters are needed to quantify the magnitude of nonpairwise additive contributions. We have also investigated the size evolution of the equilibrium structures and approximate HCl vibrational red-shifts for $\mathrm{Ar}_n\mathrm{HCl}$ clusters ($n=1-12$) utilizing the accurate pairwise additive $\mathrm{Ar}_n\mathrm{HCl}$ potential. These studies indicate qualitative structural differences for $\mathrm{Ar}_{12}\mathrm{HCl}$ and $\mathrm{Ar}_{12}\mathrm{HF}$ surrounded by one solvation shell. Specifically, for $\mathrm{Ar}_{12}\mathrm{HCl}$, the lowest energy structure consists of HCl bound to the *surface* of an Ar_{12} cluster, as opposed to the *interior* minimum energy structure predicted for $\mathrm{Ar}_{12}\mathrm{HF}$.

The availability of matrix isolation spectra for HCl in argon also makes comparison between experiment and theory possible for the condensed phase. These calculations indicate the HCl red-shift is sensitive to Ar atoms well beyond its 12 nearest neighbors in the first solvation shell, but is reasonably converged by $n_{\mathrm{shell}}\approx 4$. By way of contrast, the

red-shifts in the Ar_nHF system are mostly sensitive only to Ar atoms in direct contact with the HF chromophore, thus suggesting that a more local description of the condensed phase interactions should suffice. This work demonstrates clearly that the combination of high resolution spectroscopy of gas phase clusters with classical and/or quantum theoretical analysis on accurate pair potentials offers an interesting alternative window into solvent shell dynamics in the condensed phase environment.

Note added in proof. Since completion of this work, full 5D quantum variational calculations on $v_{HCl}=1\leftarrow 0$ vibrational red-shifts ($\approx$3.07–3.18 cm^{-1}) in Ar_2HCl have been recently reported by Ernesti and Hutson [J. Chem. Phys. **106**, 6288 (1997)] that are in reasonably good agreement with experiment (3.2236 cm^{-1}). Furthermore, their work correctly predicts a red-shift that is *decreased* from the pairwise additive results (3.329 cm^{-1}) by nonpairwise additivity in the potentials, though by roughly twofold more than experimentally observed.

ACKNOWLEDGMENT

Financial support for this research from the National Science Foundation is gratefully acknowledged. We would also like to thank Professor Zlotko Bacic for several useful discussions.

[1] D. J. Nesbitt, Chem. Rev. **88**, 843 (1988).
[2] M. A. Suhm and D. J. Nesbitt, Chem. Soc. Rev. **24**, 45 (1995).
[3] J. M. Hutson, J. Phys. Chem. **96**, 4237 (1992).
[4] J. M. Hutson, J. Chem. Phys. **96**, 6752 (1992).
[5] R. J. Le Roy and J. M. Hutson, J. Chem. Phys. **86**, 837 (1987).
[6] R. C. Cohen and R. J. Saykally, J. Chem. Phys. **98**, 6007 (1993).
[7] C. A. Schumuttenmaer, R. C. Cohen, and R. J. Saykally, J. Chem. Phys. **101**, 146 (1994).
[8] H. S. Gutowsky *et al.*, J. Chem. Phys. **86**, 569 (1987).
[9] H. S. Gutowsky *et al.*, J. Am. Chem. Soc. **109**, 5633 (1985).
[10] H. S. Gutowsky *et al.*, J. Chem. Phys. **83**, 4817 (1985).
[11] T. D. Klots *et al.*, J. Chem. Phys. **87**, 5315 (1987).
[12] T. D. Klots *et al.*, J. Chem. Phys. **87**, 4383 (1987).
[13] M. J. Elrod, J. G. Loeser, and R. J. Saykally, J. Chem. Phys. **98**, 5352 (1992).
[14] M. J. Elrod, D. W. Steyert, and R. J. Saykally, J. Chem. Phys. **95**, 3182 (1991).
[15] M. J. Elrod, D. W. Steyert, and R. J. Saykally, J. Chem. Phys. **94**, 58 (1991).
[16] M. J. Elrod *et al.*, Mol. Phys. **81**, 579 (1994).
[17] John T. Farrell, Jr. and David J. Nesbitt, J. Chem. Phys. **105**, 9421 (1996).
[18] A. McIlroy *et al.*, J. Chem. Phys. **95**, 2636 (1991).
[19] John T. Farrell, Jr., Scott Davis, and David J. Nesbitt, J. Chem. Phys. **103**, 2395 (1995).
[20] R. A. Aziz, J. Chem. Phys. **99**, 4518 (1993).
[21] A. R. Cooper and J. M. Hutson, J. Chem. Phys. **98**, 5337 (1992).
[22] L. Young and C. B. Moore, J. Chem. Phys. **81**, 3137 (1984).
[23] D. E. Mann, N. Acquita, and D. White, J. Chem. Phys. **44**, 3453 (1966).
[24] Marius Lewerenz (private communication).
[25] B. J. Howard and A. S. Pine, Chem. Phys. Lett. **122**, 1 (1985).
[26] J. K. G. Watson, J. Chem. Phys. **46**, 1935 (1967).
[27] J. M. Hutson and B. J. Howard, J. Chem. Phys. **74**, 6520 (1981).
[28] S. E. Novick *et al.*, J. Chem. Phys. **65**, 1114 (1976).
[29] S. E. Novick *et al.*, J. Chem. Phys. **59**, 2273 (1973).
[30] M. D. Marshall *et al.*, J. Chem. Phys. **83**, 4924 (1985).
[31] D. Ray *et al.*, J. Chem. Phys. **84**, 1171 (1986).
[32] R. L. Robinson, D.-H. Gwo, and R. J. Saykally, J. Chem. Phys. **86**, 5211 (1987).
[33] R. L. Robinson *et al.*, J. Chem. Phys. **87**, 5149 (1987).
[34] R. L. Robinson, D.-H. Gwo, and R. J. Saykally, J. Chem. Phys. **87**, 5156 (1987).
[35] K. L. Busarow *et al.*, Chem. Phys. Lett. **141**, 289 (1987).
[36] C. M. Lovejoy and D. J. Nesbitt, Chem. Phys. Lett. **146**, 582 (1988).
[37] B. M. Axilrod and E. Teller, J. Chem. Phys. **11**, 299 (1943).
[38] Y. Muto, Proc. Phys. Math. Soc. Jpn. **17**, 629 (1943).
[39] P. R. Herman, P. E. LaRoque, and B. P. Stoicheff, J. Chem. Phys. **89**, 4535 (1988).
[40] E. A. Colbourn and A. E. Douglass, J. Chem. Phys. **65**, 1741 (1976).
[41] R. A. Aziz, in *Inert Gases*, edited by M. L. Klein (Springer, Berlin, 1984), Vol. 34.
[42] S. Liu, Z. Bacic, J. W. Moskowitz, and R. E. Schmidt, J. Chem. Phys. **100**, 7166 (1994).
[43] S. Liu, B. Zlatko, and J. W. Moskowitz, J. Chem. Phys. **103**, 1829 (1993).
[44] S. Liu, Z. Bacic, and J. W. Moskowitz, J. Chem. Phys. **101**, 10 181 (1994).
[45] S. Liu *et al.*, J. Chem. Phys. **101**, 6359 (1994).
[46] M. Lewerenz, J. Chem. Phys. **104**, 1028 (1996).
[47] P. Niyaz, Z. Bacic, J. W. Moskowitz, and R. E. Schmidt, Chem. Phys. Lett. **252**, 23 (1996).
[48] J. M. Sperhac, M. J. Weida, and D. J. Nesbitt, J. Chem. Phys. **104**, 2202 (1996).